blood®
Regular Article

IMMUNOBIOLOGY AND IMMUNOTHERAPY

B-cell–directed CAR T-cell therapy activates CD8$^+$ cytotoxic CAR^{neg} bystander T cells in patients and nonhuman primates

James Kaminski,[1,2] Ryan A. Fleming,[1] Francesca Alvarez-Calderon,[1,3,4] Marlana B. Winschel,[1] Connor McGuckin,[1] Emily E. Ho,[5] Fay Eng,[5] Xianliang Rui,[1] Paula Keskula,[1] Lorenzo Cagnin,[1] Joanne Charles,[1] Jillian Zavistaski,[1] Steven P. Margossian,[1,3,4] Malika A. Kapadia,[1,3,4] James B. Rottman,[5] Jennifer Lane,[1,6] Susanne H. C. Baumeister,[1,3,4] Victor Tkachev,[1,3,6] Alex K. Shalek,[2,7-10,*] Leslie S. Kean,[1,3,4,*] and Ulrike Gerdemann[1,3,4,*]

[1]Division of Pediatric Hematology-Oncology, Boston Children's Hospital, Boston, MA; [2]Broad Institute of MIT and Harvard, Cambridge, MA; [3]Department of Pediatric Oncology, Dana-Farber Cancer Institute, Boston, MA; [4]Harvard Medical School, Boston, MA; [5]2seventy bio, Cambridge, MA; [6]Center for Transplantation Sciences, Massachusetts General Hospital, Boston, MA; [7]Department of Chemistry, [8]Institute for Medical Engineering & Science, and [9]Koch Institute for Integrative Cancer Research, Massachusetts Institute of Technology, Cambridge, MA; and [10]Ragon Institute of Massachusetts General Hospital, MIT and Harvard, Cambridge, MA

KEY POINTS

- **Transcriptomic analysis of NHP and patient-derived T cells following CAR T-cell infusion identified activated CAR$^-$ bystander CD8$^+$ T cells.**
- **Cytokine exposure–induced bystander-like CD8$^+$ T cells capable of T-cell receptor–independent cytotoxic killing of leukemia cells.**

Chimeric antigen receptor (CAR) T cells hold promise as a therapy for B-cell–derived malignancies, and despite their impressive initial response rates, a significant proportion of patients ultimately experience relapse. Although recent studies have explored the mechanisms of in vivo CAR T-cell function, little is understood about the activation of surrounding CAR^{neg} bystander T cells and their potential to enhance tumor responses. We performed single-cell RNA sequencing on nonhuman primate (NHP) and patient-derived T cells to identify the phenotypic and transcriptomic hallmarks of bystander activation of CAR^{neg} T cells following B-cell–targeted CAR T-cell therapy. Using a highly translatable CD20 CAR NHP model, we observed a distinct population of activated CD8$^+$ CAR^{neg} T cells emerging during CAR T-cell expansion. These bystander CD8$^+$ CAR^{neg} T cells exhibited a unique transcriptional signature with upregulation of natural killer-cell markers (*KIR3DL2*, *CD160*, and *KLRD1*), chemokines, and chemokine receptors (*CCL5*, *XCL1*, and *CCR9*), and downregulation of naïve T-cell-associated genes (*SELL* and *CD28*). A transcriptionally similar population was identified in patients after a tisagenlecleucel infusion. Mechanistic studies revealed that interleukin-2 (IL-2) and IL-15 exposure induced bystander-like CD8$^+$ T cells in a dose-dependent manner. In vitro activated and patient-derived T cells with a bystander phenotype efficiently killed leukemic cells through a T-cell receptor–independent mechanism. Collectively, to our knowledge, these data provide the first comprehensive identification and profiling of CAR^{neg} bystander CD8$^+$ T cells following B-cell–targeting CAR T-cell therapy and suggest a novel mechanism through which CAR T-cell infusion might trigger enhanced antileukemic responses. Patient samples were obtained from the trial #NCT03369353, registered at www.ClinicalTrials.gov.

Introduction

Chimeric antigen receptor (CAR) T cells are a breakthrough therapy capable of inducing remission in patients with relapsed or refractory B cell–derived malignancies.[1-4] However, despite high rates of initial response, up to 50% of responding patients eventually experience relapse.[3,4] Several studies using single-cell RNA sequencing (scRNA-seq) have identified the key transcriptional drivers of CAR T-cell success or failure.[1,5-11] However, an additional aspect of the therapeutic effect of CAR T cells, which is now gaining increasing attention, is their impact on the surrounding immune cells,[12] as well as their potential role in contributing to the antitumor response.[12]

Bystander activation was initially described in viral infections, in which T cells lacking T-cell receptors (TCRs) cognate with viral antigens were discovered to contribute to viral clearance.[13] Recent studies have found evidence of TCR–independent tumor lysis by bystander-activated T cells within the tumor microenvironment.[12,14-17] Although some phenotypic analysis has been performed to characterize bystander-activated cells in viral infections and the tumor environment, a comprehensive

transcriptomic profile to better understand the mechanisms driving their activation has been lacking.[13-15,18-20] Moreover, a recent study provided initial evidence that the infusion of CAR T cells triggers the activation of neighboring CAR^{neg} bystander T cells;[12] however, identification of the transcriptional profile of bystander-activated CAR^{neg} T cells and the mechanisms regulating their activation during CAR T-cell therapy, has remained elusive.

In this study, to our knowledge, we, for the first time, characterized an activated CD8$^+$ CAR^{neg} T-cell bystander population in both nonhuman primate (NHP) and patient samples and identified their unique transcriptional profile, including the expression of both T-cell activation markers as well as canonical natural killer-cell (NK-cell) markers. We further demonstrated that in vitro-generated or patient–derived bystander CD8$^+$ T cells can induce significant lysis of leukemic blasts in a TCR-independent manner. These findings highlight distinct bystander populations induced by CAR T-cell therapy with the potential to contribute to antileukemic control.

Methods

NHP in vivo adoptive T-cell transfer studies

The NHP experiments were approved by the University of Washington and the Biomere Institutional Animal Care and Use Committee (IACUC). Each rhesus macaque recipient received cyclophosphamide (Baxter) as lymphodepleting chemotherapy, as previously described,[21] and was infused with doses ranging from 0.6 × 10^7 to 1.2 × 10^7 CD20 CAR T cells per kg.

Patient sample collection and cryopreservation

Peripheral blood samples from pediatric patients with B-cell acute lymphoblastic leukemia (B-ALL) receiving tisagenlecleucel were collected under the Boston Children's Hospital approved clinical protocol, Precision Diagnostics in Inflammatory Bowel Disease, Cellular Therapy and Transplantation (PREDICT) (NCT03369353). Peripheral blood mononuclear cells (PBMCs) were isolated using Ficoll-Paque PLUS (GE Healthcare) gradient centrifugation and cryopreserved.

Cytokine stimulation assays

T cells from healthy donor PBMCs, obtained using a Boston Children's Hospital institutional review board approved protocol, were selected using the Pan-T-cell isolation kit (Miltenyi Biotec). T cells were plated at 200 000 cells in 96-well U-bottom plates and stimulated for 24 to 48 hours with interleukin-2 (IL-2), tumor necrosis factor alpha (TNF-α), IL-15, IL-1β, IL-12, IL-6, granulocyte-macrophage colony-stimulating factor, IL-4, IL-7, IL-18, and interferon gamma (IFN-γ). After cytokine stimulation, the cells were stained with CD3, CD4, CD8, CD160, killer cell lectin like receptor K1 (NKG2D), CD94, and CCL5 for flow cytometry analysis.

Cytotoxicity assays

Healthy donor T cells were unstimulated or stimulated with IL-15 (50 ng/mL), IL2 (500 U/mL) for 24 hours, and unstimulated patient-derived PBMCs were stained with a live/dead marker, CD3, CD4, CD8, CD94, NKG2D, and CD160. CD8$^+$ cells were sorted into NKG2D, CD160, and CD94-positive or -negative populations. Sorted T cells were cocultured with Nalm6, Nalm6 β-2-microglobulin (β2M) knockout (k/o), and Daudi cells at an effector-to-target ratio of 1:1 for 16 hours. The percentage killing was determined by the number of live Nalm6 or Daudi cells.

NHP experiments were performed according to the Guide for the Care and Use of Laboratory Animals of the National Institutes of Health, which was approved by the University of Washington, Boston Children's Hospital, and the Biomere IACUC. The IACUC specifies the infusion and sample collection of autologous CD20 targeting CAR T cells in rhesus macaques. Peripheral blood samples from pediatric patients with B-ALL receiving tisagenlecleucel were collected under the Boston Children's Hospital and Dana-Farber Cancer Institute approved clinical protocol, "PREDICT" (NCT03369353). Healthy donor samples were collected under the Boston Children's Hospital approved institutional review board protocol.

Further experimental details and scRNA-seq analysis are found in the supplemental Methods, available on the *Blood* website.

Results

CD20 CAR T-cell expansion results in activation of CD8$^+$ but not CD4$^+$ CAR^{neg} T cells in NHP

We used flow cytometry, scRNA-seq, and single-cell TCR-sequencing (scTCR-seq) to identify expanded CAR^{neg} T-cell bystander-activated cells in the peripheral blood after CD20-CAR T-cell infusion in an NHP model.[21] This model recapitulates the efficacy and toxicity of human CAR T cells, including CAR T-cell expansion and the induction of B-cell aplasia through CAR T-cell–mediated killing, as demonstrated previously,[21] within an immunologically analogous animal system.

The experimental strategy used for a representative NHP, R.315, to obtain detailed sampling and measurements of bystander T cells is outlined in Figure 1A. This included baseline "preinfusion T-cell" samples, cells sampled from the infusion product, cells from the peripheral blood sampled at peak CAR T-cell expansion (day 10), and the start of CAR T-cell contraction (day 14). CAR^{pos} and CAR^{neg} T cells were purified flow cytometrically using the CD20-CAR–directed rituximab antibody. Figure 1B demonstrates both CAR T-cell expansion/contraction and B-cell aplasia in R.315. At peak expansion, on day 10, 39% of all CD3$^+$ cells in R.315 were CAR T cells, consistent with CAR T-cell expansion in our cohort of NHP CAR T-cell recipients (R.301 to R.304, for which 20%-88% of total CD3$^+$ T cells were CAR$^+$ at peak expansion; supplemental Table 1).[21]

To further characterize the CAR^{pos} and CAR^{neg} cells emerging after CAR T-cell infusion, we performed 5′ scRNA-seq and scTCR-seq and obtained 11 392 CAR^{neg} and 9340 CAR^{pos} T cells from R.315 (Figure 1C-F; supplemental Figure 1). Figure 1C demonstrates the separation between the CAR T-cell product and the pre- and postinfusion time points comprising both CAR^{pos} and CAR^{neg} T cells in the blood from R.315 via a uniform manifold approximation and projection (UMAP) plot. Figure 1D displays CAR^{pos} (red) and CAR^{neg} (blue) T cells based on flow cytometrically sorted populations.[21] Figure 1E displays

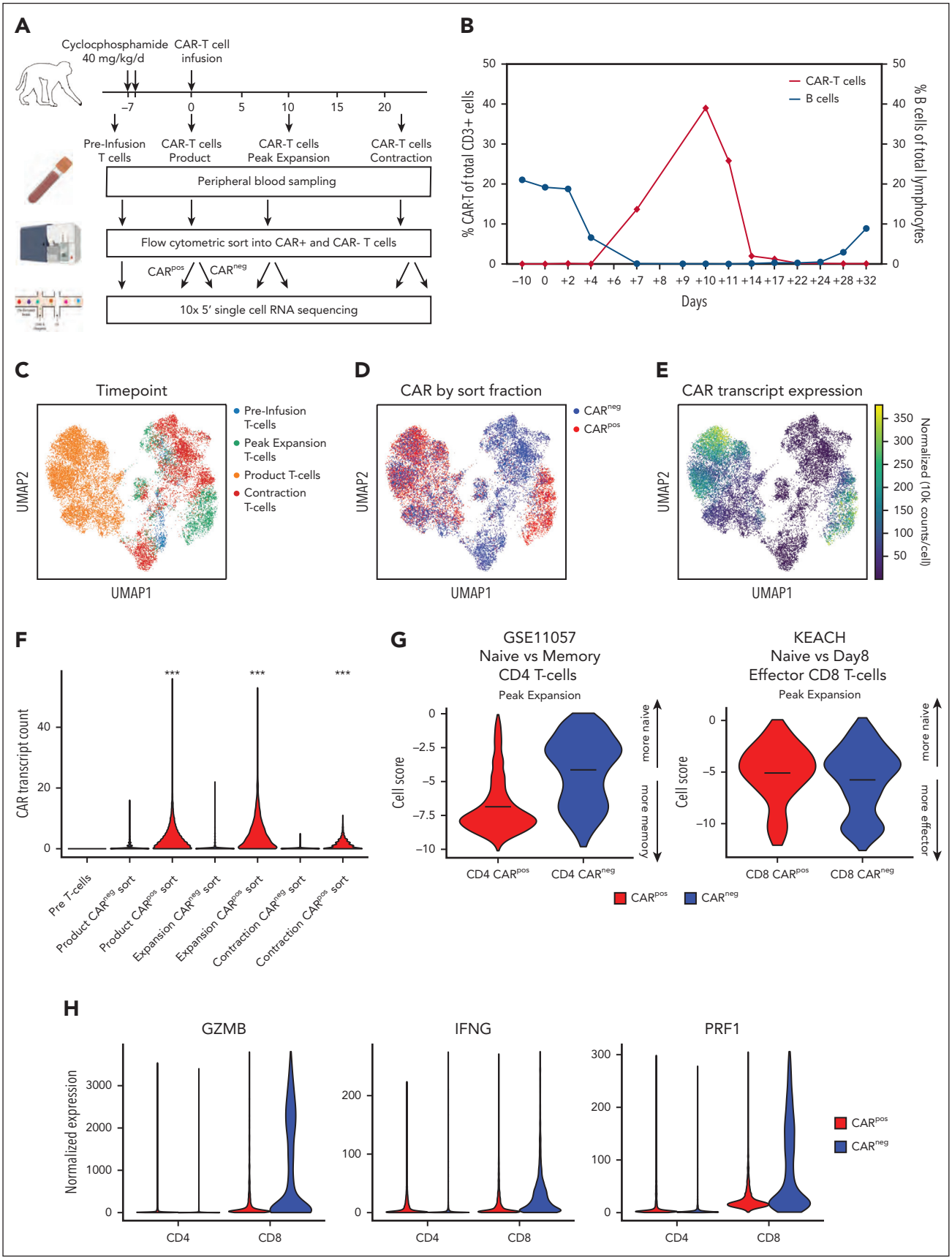


Figure 1. NHP model of CAR T-cell therapy reveals CD8^{+} CAR^{neg} T cells with an activation signature. (A) Schematic of sample preparation: T cells, CAR^{pos}, and CAR^{neg} cells were flow cytometrically sorted before infusion, from the product, at day 10 (peak expansion) and day 14 (the start of CAR T-cell contraction), and prepared for scRNA-seq

normalized expression of the CAR transcript. A comparison of Figure 1D-E confirmed high congruency between flow cytometric and transcriptomic identification of CAR^{pos} T cells. Figure 1F shows the unadjusted CAR transcript count in each sorted population, with significantly higher levels of the CAR transcript in the CAR^{pos} cells than in CAR^{neg} (the Wilcoxon rank sum test, $P < .001$), again confirming our ability to identify both CAR^{pos} and CAR^{neg} T cells with high accuracy.

Previous studies have indicated that bystander activation primarily occurs in $CD8^+$ T cells.[13-15] We assessed the state of peak expansion of T cells using the decoupleR[22] package to score the transcriptome of cells with canonical signatures: for CD4 cells, a memory-associated T-cell signature (the GSE11057 gene set[23]), and for $CD8^+$, an effector-associated T-cell signature (the KEACH naïve vs day 8 effector $CD8^+$ T-cell gene set[24]). Figure 1G demonstrates a substantial difference between CAR^{pos} and CAR^{neg} $CD4^+$ T cells (CAR^{pos}, −6.86; CAR^{neg}, −4.11; $P < .001$ using the Welch t test), but in contrast, CAR^{neg} and CAR^{pos} $CD8^+$ T cells acquired a similar effector-like signature, suggestive of activation of CAR^{neg} bystander $CD8^+$ T cells. Consistent with this effector signature, both $CD8^+$ CAR^{pos} and CAR^{neg} cells demonstrated enrichment for the genes encoding granzyme B, perforin 1, and IFN-γ at the time of peak CAR T-cell expansion (Figure 1H). The enrichment of these genes was slightly higher in $CD8^+$ CAR^{neg} than in $CD8^+$ CAR^{pos} T cells, likely because of the smaller fraction of $CD8^+$ CAR^{pos} T cells in this animal, with a predominance of $CD4^+$ CAR^{pos} T cells. These findings indicate that bystander activation predominantly occurred within $CD8^+$ CAR^{neg} T-cell populations.

scRNA-seq identifies the transcriptional program of bystander-activated $CD8^+$ T cells after CAR T-cell infusion

To deepen our understanding of the transcriptional signature of NHP $CD8^+$ CAR^{neg} bystander T cells, we performed additional analyses of the scRNA-seq data from R.315. Figure 2A demonstrates the Leiden clustering of both CAR^{pos} and CAR^{neg} T cells, in which 16 unique cell clusters were identified. Four clusters were enriched for $CD8^+$ CAR^{neg} T cells (cluster numbers 4, 5, 10, and 14; Figure 2B-C). As shown in Figure 2C and supplemental Table 2, clusters 4, 10, and 14 demonstrated the expression of genes encoding selected effector molecules (IFN-γ and IL-2), cytolytic molecules (granzyme A, granzyme B, granzyme M), and several canonical NK-cell markers (NKG2D and killer cell lectin like receptor D1).

To determine which $CD8^+$ CAR^{neg} cluster(s) may be enriched in bystander cells associated with CAR T-cell expansion, we investigated the time point composition of clusters 4, 5, 10, and 14. Figure 2D and supplemental Table 3 demonstrate that clusters 4, 5, and 10 included a substantial proportion of cells obtained at the preinfusion time point, and therefore were not exclusively identified during CAR T-cell expansion. In contrast, CAR^{neg} $CD8^+$ T-cell cluster 14 was almost entirely composed of T cells identified after infusion, suggesting that the effector/activation status of cells in this cluster is closely linked to CAR T-cell expansion. Cluster 14 also demonstrated high TCR diversity (supplemental Figure 2A-B), consistent with these cells being composed of polyclonal T cells. Therefore, further computational analysis focused on cluster 14.

To develop a transcriptional signature for activated bystander CAR^{neg} $CD8^+$ T cells, we used the single-cell variational inference (scVI) differential expression test[25,26] and identified a distinct transcriptional signature ("bystander signature 1") of genes that were differentially expressed (DE) in cluster 14 vs all other cells. Applying a false discovery rate cutoff of 0.05 resulted in a list of 43 upregulated and 29 downregulated genes in these activated CAR^{neg} $CD8^+$ T cells (Table 1). Figure 2E, labeled with the top 6 up- and downregulated genes, demonstrates that this signature included upregulation of T-cell effector and NK-cell-associated genes, including *CD160* and *KIR3DL2*, and downregulation of naïve T-cell-associated genes, including *SELL*, *CD28*, and *CCR7* (Table 1; Figure 2E). This is consistent with a phenotype previously associated with highly activated bystander $CD8^+$ T cells during viral infections and in the tumor microenvironment.[13-15,18-20] Indeed, an analysis of the 43 upregulated DE genes underscored this conclusion, with 40% of these genes being associated with effector T-cell and/or NK-cell function (Figure 2F). The differential expression test used for bystander signature 1 measured the overall differences between all bystander $CD8^+$ T cells and all nonbystander T cells (both $CD4^+$ and $CD8^+$) in our data set. In addition, we conducted additional bystander vs nonbystander DE tests and developed 2 additional bystander signatures ("bystander signature 2, 3"; supplemental Figure 2C-D; supplemental Table 4) that demonstrated substantial overlap, underscoring the consistency of these analyses in identifying bystander-defining genes. Finally, we created a minimal gene list, "bystander signature 4" (supplemental Figure 2C), using 5 genes (*CD8A, CD160, KLRK1* [NKG2D], *KLRD1* [CD94], and *CCL5*) that are each highly expressed in the bystander cluster and that are also amenable to flow cytometric identification. Underscoring the rigor of our cluster identification, the CAR^{neg} bystander cluster was distinct across multiple levels of clustering resolution (supplemental Figure 2E).

Bystander T cells arise from the recipient's peripheral blood $CD8^+$ T cells after CAR T-cell infusion

To determine whether $CD8^+$ CAR^{neg} bystander T cells expanded from the infused product or T cells in the recipient, we performed scTCR-seq and assembled TCRs[27] from R.315, assigned them to clones, assessed their number and diversity, and determined their similarity across samples (supplemental Figure 2A-B). We used the Morisita index[28] to examine the degree of clonal overlap between cluster 14 clones and clones

Figure 1 (continued) and scTCR-seq. (B) CAR T-cell expansion and B-cell aplasia were tracked in animal R.315. (C) Uniform manifold approximation and projection (UMAP) with Leiden clustering of the scRNA-seq data set, colored by the time point. (D) UMAP of the scRNA-seq data set colored by flow cytometrically sorted CAR^{pos} and CAR^{neg} cells. (E) UMAP of the scRNA-seq data set, colored by the normalized CAR transcript counts. (F) Unadjusted CAR transcript counts in the sorted CAR^{pos} and CAR^{neg} populations. (G) decoupleR weighted sum (WSUM) analysis of a naïve vs memory gene signature in CD4+ CAR^{pos} and CAR^{neg} T cells and a naïve vs effector gene signature in $CD8^+$ CAR^{pos} and CAR^{neg} T cells, with the analysis performed with cells isolated at the time of peak expansion. (H) Violin plots of normalized expression of the $CD8^+$ effector molecules granzyme B (GZMB), IFN-γ, and perforin 1 (PRF1) in $CD4^+$ and $CD8^+$ CAR^{pos} and CAR^{neg} T cells.

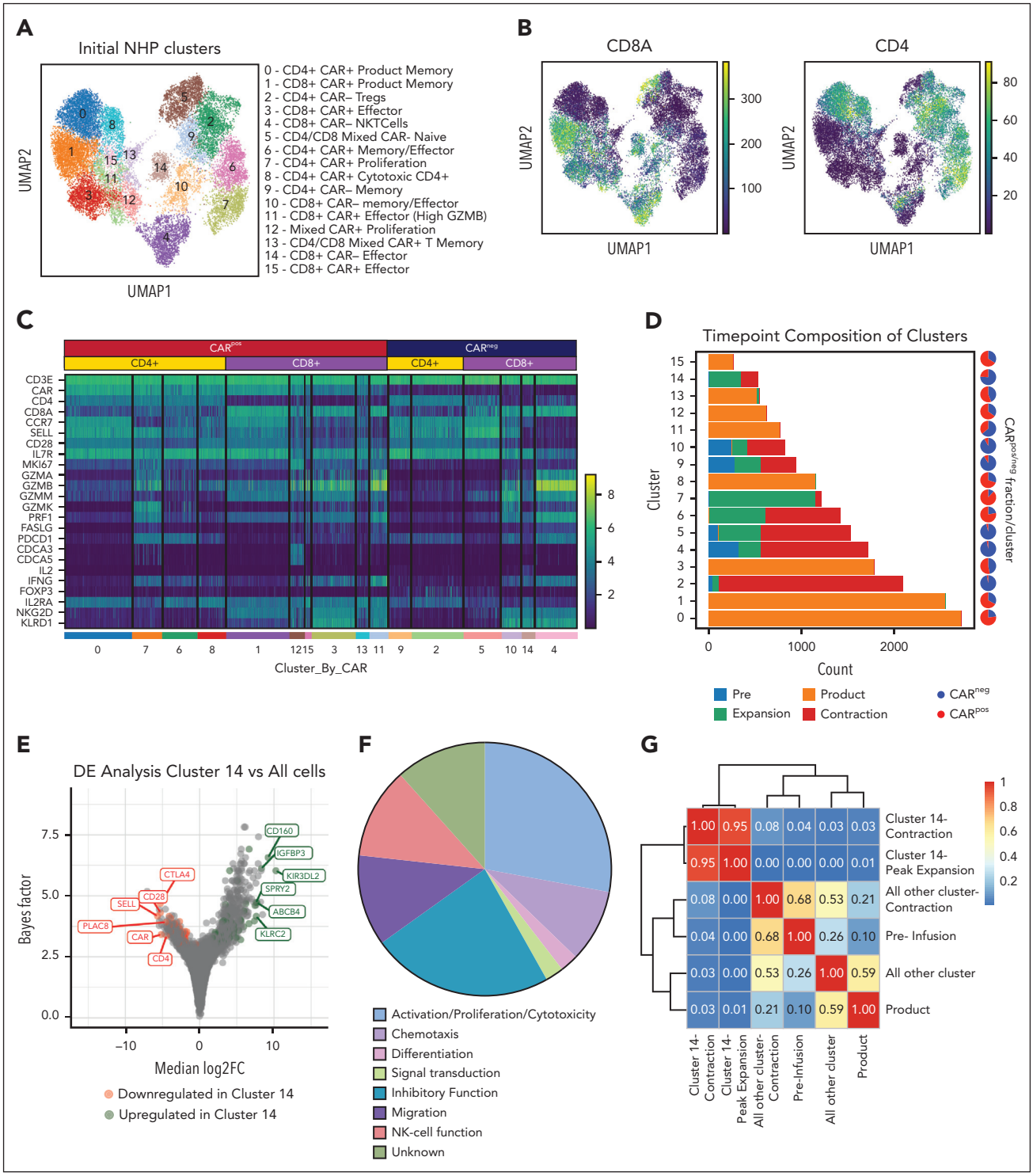


Figure 2. Identification of CD8$^+$ bystander signature in the NHP model. (A) UMAP with Leiden clustering from NHP recipient R.315. Sixteen clusters are denoted by colors and labeled with inferred cell states. (B) UMAP with normalized CD8a and CD4 expression. (C) Heat map demonstrating normalized and log-scaled expression of selected T-cell activation, effector, and known bystander genes. (D) Cluster composition based on the time point of sample collection. (E) Differential expression of the bystander cluster (cluster 14) vs all other clusters in the data set. The top 6 upregulated (green) and downregulated (red) genes by median log2 fold change are labeled. (F) The 42 genes that exhibited upregulation in bystander signature 1 were classified based on their proposed function in T cells. (G) Heat map of Morisita index for all samples, comparing cluster 14 cells (at contraction and peak expansion) with all other cells using the clonotype ID inferred by Cell Ranger to group cells into clones.

Table 1. Genes defining the bystander-specific gene signature "bystander signature 1"

Upregulated genes		Downregulated genes	
Gene name (human ortholog)	**Log fold change**	**Gene name**	**Log fold change**
KIR3DL2	10.26	*EZH2*	−1.73
CD160	9.21	*SLC2A3*	−1.78
IGFBP3	8.31	*GNG2*	−1.83
ABCB4	7.72	*LYST*	−1.97
ENSMMUG00000050862 (KLRC2)	7.62	*LTB*	−1.98
SPRY2	7.58	*TESPA1*	−1.98
XCL1	7.44	*SATB1*	−2.11
CCL5	7.36	*CCR7*	−2.16
NUGGC	6.65	*ICOS*	−2.24
ENSMMUG00000063583 (GNLY)	6.63	*SIT1*	−2.25
ENSMMUG00000013779	5.95	*DUSP16*	−2.38
CCR9	5.93	*SH2D1A*	−2.41
KLRD1	5.52	*PTPRJ*	−2.43
ENSMMUG00000054501 9 (TRGV)	5.47	*H1-3*	−2.52
CD101	5.04	*SLFN12L*	−2.71
PPP2R2B	4.89	*PDE4B*	−2.71
SERPINB6	4.61	*PGAP1*	−2.72
PLCG2	4.55	*CFP*	−2.75
ENSMMUG00000057791 (TRDV)	4.54	*ANTXR2*	−2.88
LAT2	4.48	*GPR183*	−2.93
ANK3	4.16	*SPOCK2*	−3.37
THAP6	4.03	*MT1E*	−3.46
JAKMIP2	4.02	*S1PR1*	−3.89
THY1	3.96	*LEF1*	−4.09
MATK	3.87	*TOB1*	−4.13
ENTPD1	3.71	*CD4*	−4.47
ENSMMUG00000032338 (SMIM10)	3.62	*PLAC8*	−4.59
TIGIT	3.59	*CD28*	−5.29
OTUD5	3.52	*SELL*	−5.68
FCRL6	3.44	—	—
NCALD	3.32	—	—
NKG7	3.17	—	—
ITGA1	3.03	—	—

Gene list for bystander signature 1. Listed genes are DE (up- and downregulated) in cluster 14 compared with all other cells in the data set for animal R.315.

Table 1 (continued)

Upregulated genes		Downregulated genes	
Gene name (human ortholog)	**Log fold change**	**Gene name**	**Log fold change**
NR3C2	2.88	—	—
DAPK2	2.79	—	—
SPINK2	2.73	—	—
PRR29	2.73	—	—
STX3	2.34	—	—
RIN3	2.32	—	—
NR4A1	2.27	—	—
S100A6	2.23	—	—
UBASH3B	2.13	—	—
CPQ	2.11	—	—

Gene list for bystander signature 1. Listed genes are DE (up- and downregulated) in cluster 14 compared with all other cells in the data set for animal R.315.

identified in the infused product at the time of peak CAR T-cell expansion and in the CAR T-cell contraction phase. This analysis identified a high degree of clonal overlap between cluster 14 CAR^{neg} bystander T cells present at the time of CAR T-cell peak expansion and contraction, but much less overlap between this cluster and either the preinfusion T cells or infused product (Figure 2G). These data support a model wherein most CAR^{neg} bystander cells arise from peripheral blood $CD8^+$ T cells that acquire this unique phenotype in the setting of CAR T-cell expansion.

Bystander T cells are identified in 4 additional NHP recipients of CD20-CAR T cells

To determine whether cells bearing the bystander signature were present in other NHP recipients of CAR T cells, we applied bystander signature 1 to a validation cohort of 4 additional recipients.[21] The clinical and CAR T-cell course for these animals has been previously described,[21] with CAR T-cell expansion comparable with that of the animal R.315 (supplemental Table 1). For this analysis, we again performed 5′ scRNA-seq on preinfusion T cells and CAR^{pos} and CAR^{neg} T cells from the product, peripheral blood at the time of CAR T-cell peak expansion, and the start of CAR T-cell contraction (supplemental Figure 3A-C). Figure 3A demonstrates the Leiden clustering of 29 050 CAR^{neg} and 5480 CAR^{pos} derived from animals R.301, R.302, R.303, and R.304, with 24 distinct clusters identified (supplemental Tables 5 and 6).

We next applied bystander signature 1 to these clusters using decoupleR to score the cells. As shown in Figure 3B, cluster 22 exhibited a much higher bystander signature 1 score than the other clusters, identifying the cluster as likely consisting of bystander T cells (cluster 22 signature score vs score on all other cells; the Welch *t* test; $P < .001$). Cluster 22 also achieved the highest signature scores when applying bystander signatures 2-4 (supplemental Figure 3D). Figure 3C heat map displays the row-scaled normalized expression of the top 10 upregulated and bottom 10 downregulated genes for bystander signature 1, illustrating the alignment of cluster 22 with this signature. A plot of all available genes in the data set shared by the signature (supplemental Figure 4A) showed similar concordance. Figure 3D demonstrates that cluster 22 is composed of cells from all 4 animals, albeit with 2 animals dominating the cluster (R.303 and R301), and with most cells (95%) coming from the maximal expansion and contraction time points (Figure 3E), consistent with the findings from R.315 (Figure 2).

Bystander-activated T cells are present in patients after tisagenlecleucel infusion

To determine whether $CD8^+$ CAR^{neg} bystander T cells were also present in patients receiving CAR T cells for B-ALL, we used samples from 6 pediatric patients who received tisagenlecleucel (supplemental Table 7). We obtained 11 555 total T cells from the CAR T-cell products, 9073 sorted CAR^{pos}, and 14 249 sorted CAR^{neg} T cells from the peripheral blood collected on day +6 after infusion (Figure 4A-C). We then performed 5′ scRNA-seq and Leiden clustering, identifying 15 distinct clusters (Figure 4B; supplemental Tables 8 and 9).

To identify potential bystander T-cell clusters, we focused on $CD8^+$ clusters with >50% CAR^{neg} T cells and <1% T-cell clones from the infused cell product and identified clusters #0, 12, and 13 (Figure 4D). Clusters 5, 8, and 9 were also composed of <1% T-cell clones from the infused product, but these clusters comprised $CD4^+$ T cells. We scored cells from $CD8^+$ T-cell clusters #0, 12, and 13 using bystander signature 1. (Figure 4E; supplemental Figure 5D). The mean scores for bystander signature 1 in these clusters were cluster 0: 5.37, cluster 12: 2.82, and cluster 13: 0.44. Using the Welch *t* tests to test whether the mean bystander signature 1 score was greater in each cluster vs the mean of the remaining cells, we found that clusters 0 and 12

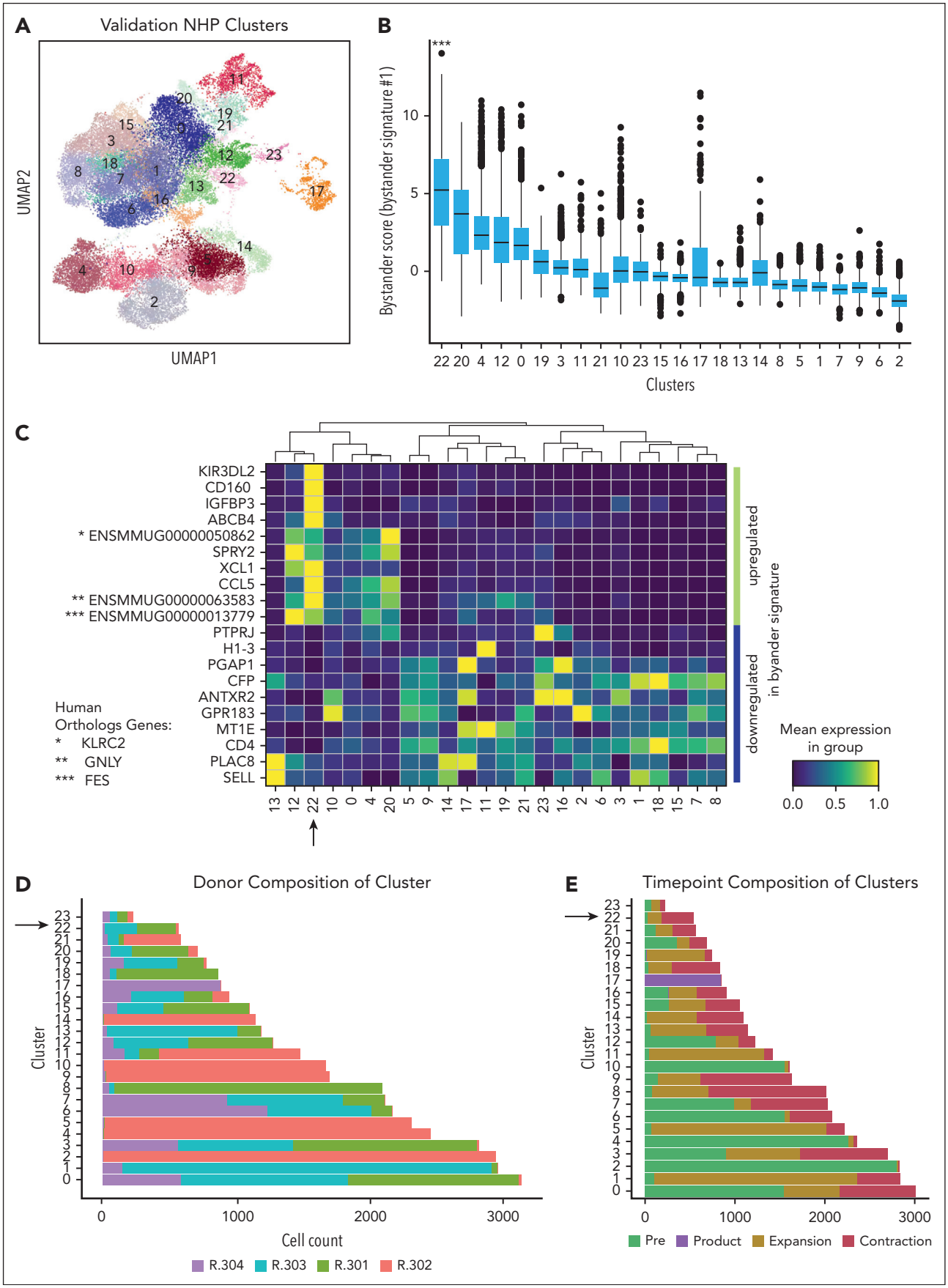

A
Validation NHP Clusters
UMAP2
UMAP1
B
Bystander score (bystander signature #1)
Clusters
C
KIR3DL2
CD160
IGFBP3
ABCB4
* ENSMMUG00000050862
SPRY2
XCL1
CCL5
** ENSMMUG00000063583
*** ENSMMUG00000013779
PTPRJ
H1-3
PGAP1
CFP
ANTXR2
GPR183
MT1E
CD4
PLAC8
SELL
Human Orthologs Genes:
* KLRC2
** GNLY
*** FES
upregulated in byander signature
downregulated
Mean expression in group
D
Donor Composition of Cluster
Cluster
Cell count
R.304
R.303
R.301
R.302
E
Timepoint Composition of Clusters
Cluster
Pre
Product
Expansion
Contraction

Figure 3.

each were significantly enriched ($P < .001$) for bystander signature 1, but that cluster 13 was not ($P = 1.0$; Figure 4D-E). Although cluster 0 comprised cells from all patients, it was predominantly populated by cells from patient number (Pt) Pt-007 (77.5%), whereas cells in cluster 12 were distributed more equally across multiple patients (Figure 4F). To ensure that Pt007 did not solely influence the identification of clusters 0 and 12 as bystander clusters, we performed a validation analysis in which data from Pt007 were excluded. Importantly, even after removing Pt007 from the analysis, both cluster 0 and cluster 12 continued to be significantly enriched for bystander signature 1 (supplemental Figure 5E) when using the Welch *t* tests.

The analysis depicted in Figure 4 includes the patient identification number (ID) as a batch term to account for patient-specific clusters. Repeat analysis conducted without including individual patient IDs as a batch term yielded similar results (supplemental Figure 6; supplemental Tables 10-13). These results suggest an overlapping transcriptional signature of bystander cells between NHP and patients.

Notably, Shannon diversity analysis of the $CD8^+$ CAR^{neg} bystander cells (clusters 0 and 12) vs nonbystander cells (cluster 13) demonstrated a lower clonal diversity in the bystander clusters within each patient (Hutcheson *t* test within each patient, all $P < 0.001$) (Figure 4G), which was driven by the expansion of several large clones (supplemental Tables 14 and 15). Although some CDR3 regions of these large clones were commensurate with published cytomegalovirus or Epstein-Barr virus-specific TCRs,[29,30] most clones in this cluster had unknown cognate antigens.

Bystander activation is induced by the gamma cytokines, IL-2 and IL-15

The identification of $CD8^+$ bystander CAR^{neg} T cells in both NHP and patients prompted us to explore the mechanisms that might contribute to their activation. In viral infection models, the stimulation of bystander T cells with cytokines has been proposed as the major activating mechanism.[13] To test this hypothesis in vitro, we exposed 7 human healthy donor T cells to cytokines that have previously been documented to be elevated after CAR T-cell infusion.[31,32] These include IL-6, IFN-γ, granulocyte-macrophage colony-stimulating factor, IL-2, IL-15, IL-7, IL-18, IL-12, IL-4, IL-1β, and TNF-α. We determined whether exposure to these cytokines would increase the expression of some of the markers identified on bystander CAR^{neg} $CD8^+$ T cells, including CD8, CD160, NKG2D, and CCL5 (Figure 5A). Figure 5B demonstrates that only stimulation with the gamma cytokines IL-2 and IL-15 was able to increase the expression of CD160, NKG2D, and CCL5 in $CD8^+$ T cells significantly (paired *t* test; $P < .03$), consistent with the acquisition of the bystander $CD8^+$ phenotype (termed "bystander-phenotype-positive" $CD8^+$ T cells). Notably, TCR stimulation with CD3/CD28-coated beads did not result in the evolution of bystander-phenotype-positive $CD8^+$ T cells, suggesting that direct TCR stimulation is not responsible for generating this cell population. Titration of IL-2 (0-1000 U/mL) and IL-15 (0-50 ng/mL) in n = 3 donor samples demonstrated a dose-dependency of the expression of the bystander markers CD8, CD160, NKG2D, and CCL5. Addition of 500 U/mL IL-2 and 50 ng/mg IL-15 resulted in the largest population of $CD8^+$ T cells expressing the bystander markers CD8, CD160, CCL5, and NKG2D (15.5% ± 6.6 and 16.1% ± 5.4, respectively) when compared with all other conditions (Figure 5C-D).

Bystander-phenotype-positive $CD8^+$ T cells show enhanced leukemic cell lysis

To assess whether bystander-phenotype-positive $CD8^+$ T cells could potentially participate in tumor control, healthy donor primary human $CD8^+$ T cells were activated with IL-15, which has previously been reported to induce bystander activation in various contexts,[13,33] and then flow-sorted based on the expression or absence of the bystander markers NKG2D, CD94, and CD160 (Figure 6A). Bystander-phenotype-positive and -negative $CD8^+$ T cells were then cocultured with the wild-type B-ALL cell line, Nalm6 (Figure 6B). Evaluation of live wild-type Nalm6 cells by flow cytometry 16 hours after coculture revealed a significantly higher degree of tumor killing by bystander-phenotype-positive compared with -negative $CD8^+$ T cells (81.0 ± 5.7% killing vs 58.2 ± 9.7% killing; n = 7; paired *t* test; $P < .01$; Figure 6B). To assess whether killing was TCR-dependent or TCR-independent, unstimulated, as well as IL-15– and IL-2–stimulated and sorted bystander-phenotype-positive and -negative $CD8^+$ T cells were then cocultured with β2M knockout Nalm6 cells (lacking major histocompatibility complex-I surface expression). Higher target cell lysis of β2M knockout Nalm6 was observed when these target cells were cocultured with IL-15 stimulated bystander-phenotype-positive $CD8^+$ T cells (85.4 ± 9.0% killing vs 57.5.9 ± 4.7% killing by bystander-phenotype-negative $CD8^+$ T cells; n = 5; paired *t* test; $P < .01$), consistent with a TCR–independent cytotoxic mechanism (Figure 6C). Notably, unstimulated $CD8^+$ T cells demonstrated significantly lower target lysis of β2M knockout Nalm6 cells (28.1 ± 4.0% killing) than IL15-stimulated bystander-phenotype-negative $CD8^+$ T cells (57.5 ± 4.7%; n = 3; $P < .01$; unpaired *t* test). The target killing by unstimulated $CD8^+$ T cells was not significantly different when compared with IL-2 stimulated bystander-phenotype-negative $CD8^+$ T cells (38.7 ± 6.7% killing; n = 3; $P = .1$; paired *t* test). This could indicate some background killing by IL-15–stimulated bystander-phenotype-negative $CD8^+$ T cells. The difference in target lysis between IL-2–stimulated bystander-phenotype-positive vs bystander-phenotype-negative $CD8^+$ T cells was not significantly different but showed a trend toward increased lysis by bystander-phenotype-positive $CD8^+$ T cells (38.7 ± 6.7% killing vs 58.4 ± 10.2% killing, n = 3; $P = .067$).

To validate these findings with an additional B-cell malignancy cell line, we assessed the target killing of the CD19-expressing, β2M-negative Daudi lymphoma cell line by bystander-phenotype-positive and -negative $CD8^+$ T cells. Again, we observed a significantly higher target lysis by IL15–stimulated

Figure 3. Bystander CAR T cells can be detected in a validation cohort of 4 additional NHP. (A) UMAP with shared nearest-neighbor clustering across 4 additional animals, colored to identify 23 transcriptional clusters. (B) Bystander score determined by applying bystander signature 1 to each cluster using decoupleR. (C) Heat map of row-scaled normalized expression averaged across each cluster for the top 10 upregulated and downregulated genes identified in bystander signature 1. (D) Composition of each cluster by animal, with an arrow highlighting cluster 22, the cluster with the highest signature score when applying bystander signature 1. (E) Composition of clusters based on sample collection time point, with an arrow highlighting cluster 22, the cluster with the highest signature score when applying bystander signature 1.

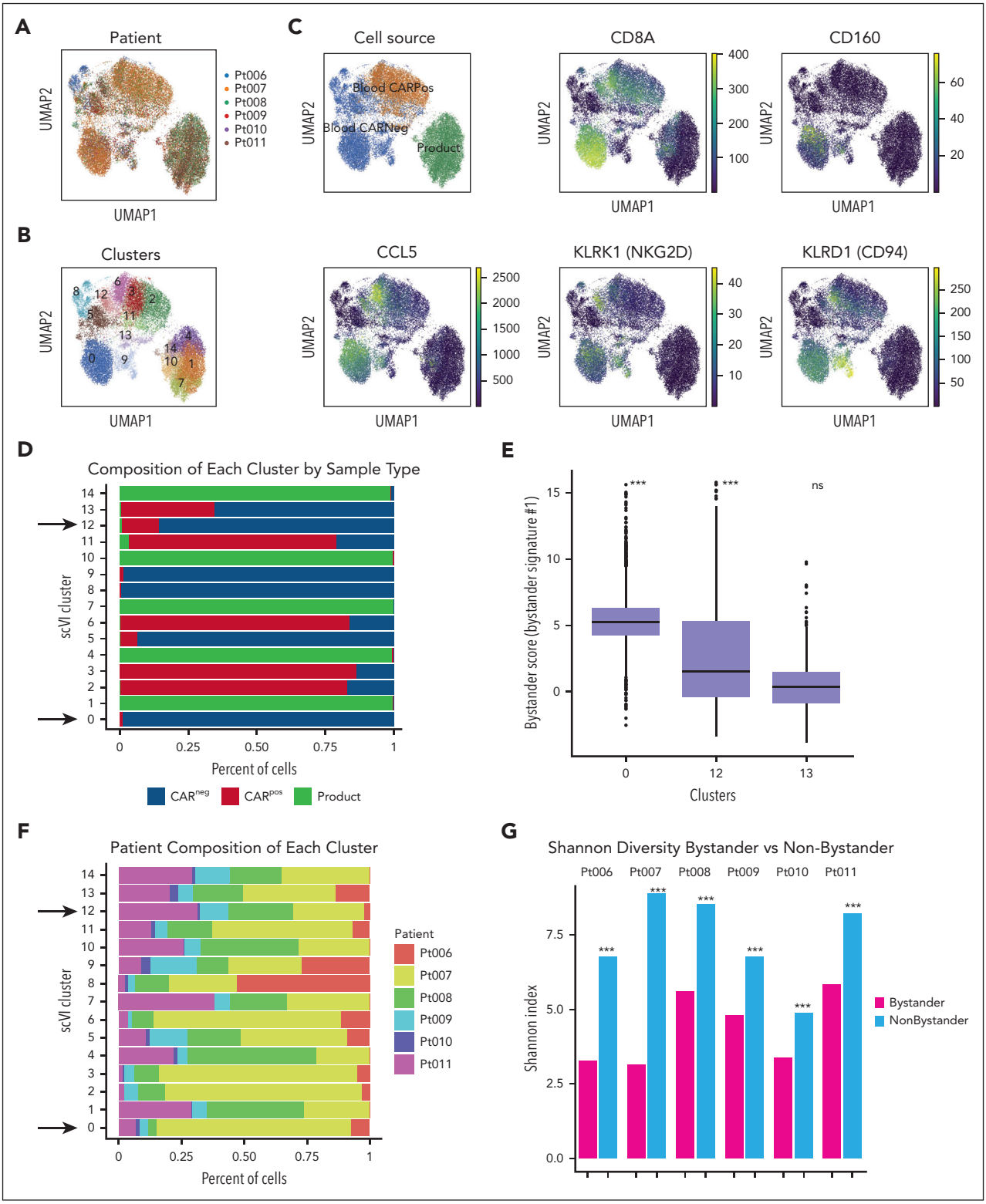


Figure 4. Identification of CD8^{+} CAR^{neg} bystander T cells in patients after tisagenlecleucel infusion. (A) UMAP of scRNA-seq data from 6 pediatric patients after tisagenlecleucel, colored by patient ID. (B) UMAP with shared nearest-neighbor clustering across all patients, colored by 15 transcriptional clusters. (C) UMAP colored by cell source, as well as normalized expression of genes from bystander signature 4 (CD8, CD160, CCL5, KLRK1 [NKG2D], and KLRD1 [CD94]). The product was not cytometrically sorted into CAR^{pos} and CAR^{neg} T cells and therefore contained a mixed population of CAR^{pos} and CAR^{neg} T cells. (D) Composition of clusters by cell source, with an arrow highlighting clusters 0 and 12, which were enriched for bystander signature 1. (E) Bystander score determined by applying bystander signature 1 to each CD8^{+} CAR^{neg} cluster using decoupleR. (F) Composition of clusters by patient ID, with arrows highlighting clusters 0 and 12, which were enriched for bystander signature 1. (G) Shannon diversity of T-cell clones in bystander clusters 12 and 0 vs all CD8^{+} CAR T cells in each patient.

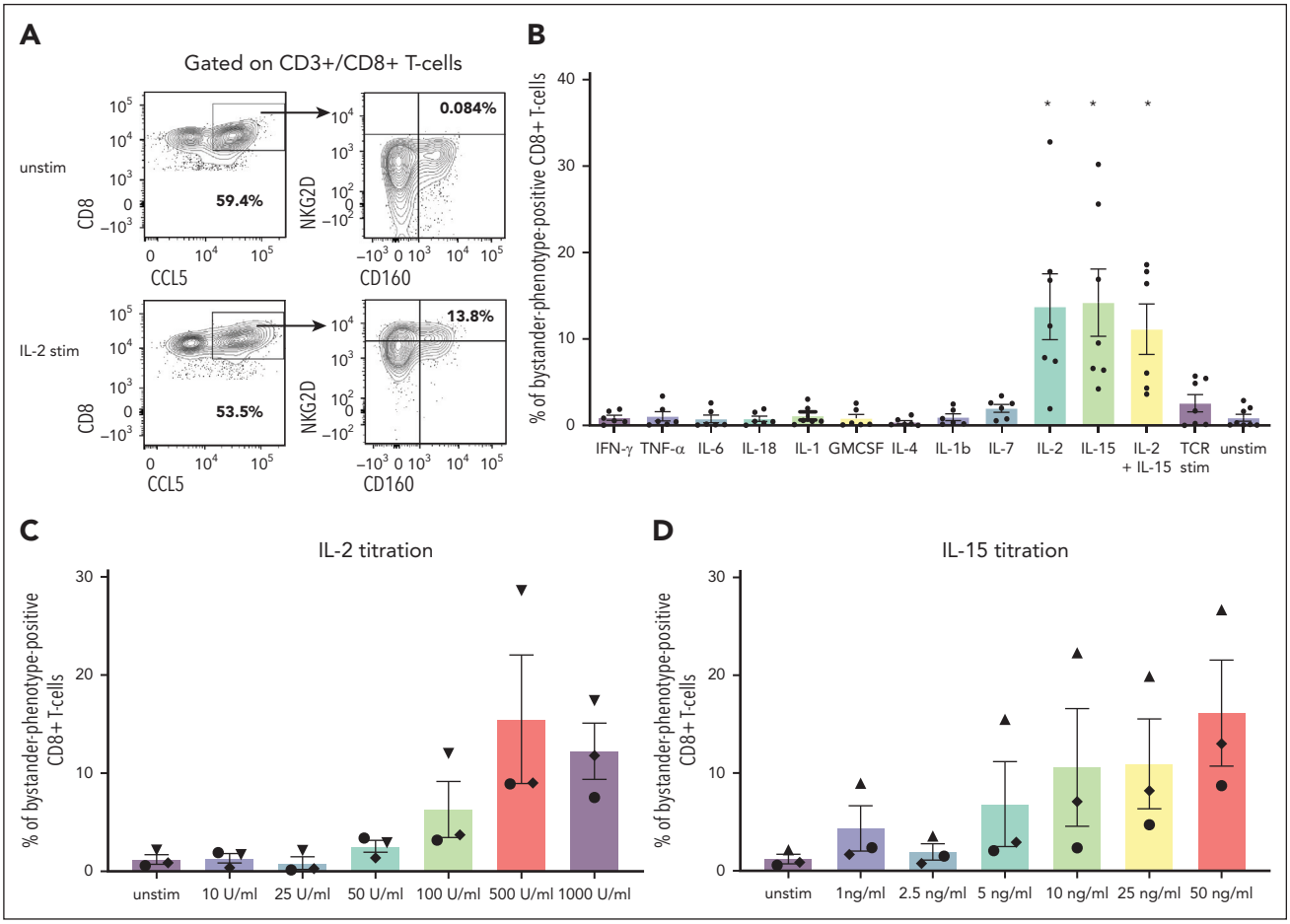


Figure 5. Stimulation of primary human T cells with gamma cytokines IL-15 or IL-2 generates cells with a bystander phenotype. (A) Representative flow plots demonstrating the gating strategy used to identify T cells expressing the bystander markers CD8, CD160, NKG2D, and CCL5 in unstimulated cells and cells stimulated with IL-2. Cells were gated on $CD3^+/CD8^+$ double-positive T cells and subsequently gated on bystander markers CCL5, NKG2D, and CD160. CD8/CCL5 double-positive cells were assessed for the expression of the bystander marker of NKG2D and CD160. (B) The percentage of total bystander-phenotype-positive $CD8^+$ T cells after stimulation with cytokine release syndrome (CRS)-associated cytokines and a paired *t* test was used for statistical analysis. (C) Percentage of total bystander-phenotype-positive $CD8^+$ T cells with the bystander phenotype after titration of IL-2 and (D) IL-15. Stim, stimulated; unstim, unstimulated.

bystander-phenotype-positive than -negative $CD8^+$ T cells (81.2 ± 3.6% killing vs 55.3 ± 7.8% killing; n = 3; $P < .03$; Figure 6D).

To determine whether bystander-activated $CD8^+$ T cells isolated from patients who had received tisagenlecleucel could also effectively lyse leukemic target cells, samples obtained on days 6 to 9 after tisagenlecleucel infusion from Pt006 and Pt007 were assessed for their fraction of bystander-phenotype-positive $CD8^+$ T cells. Pt007 exhibited higher CAR T-cell expansion than Pt006 (34.7% vs 4.64%; Figure 6E, left panel), which was associated with a larger fraction of bystander-phenotype-positive $CD8^+$ T cells (8.8% vs 5.1%; Figure 6E, right panel). Bystander-phenotype-positive and -negative T cells from Pt007 were sorted flow cytometrically and each population was cocultured with β2M knockout Nalm6 cells. Bystander-phenotype-positive $CD8^+$ T cells demonstrated higher killing of β2M knockout Nalm6 target cells (40.1 ± 2.1%) than bystander-phenotype-negative $CD8^+$ T cells (3.4 ± 5.4%; 3 technical replicates; Figure 6F). These findings demonstrate that bystander-phenotype-positive $CD8^+$ T cells can be detected in patients and that they exhibit enhanced cytotoxic function against the Nalm6 B-ALL–derived β2M knockout cell line when compared with bystander-phenotype-negative $CD8^+$ T cells.

Discussion

This study provides an initial comprehensive description and analysis of CAR^{neg} bystander T cells that become activated in the context of leukemia–targeting CAR T-cell infusions. We demonstrated that B-cell–directed CAR T-cell infusion results in bystander activation of $CD8^+$ T cells in NHP and patients receiving tisagenlecleucel. We further identified bystander-specific gene signatures, which were enriched for genes involved in T-cell activation and effector function and which included several canonical NK-cell-associated genes. Furthermore, we demonstrated that exposure to IL-15 and IL-2 could induce bystander activation and that in vitro activated and patient–derived bystander-phenotype-positive $CD8^+$ T cells have the potential to kill leukemic cells in a TCR-independent manner.

T-cell bystander activation has been studied in viral infections, including hepatitis B,[34,35] Influenza,[36] cytomegalovirus, [19] and HIV.[37,38] In these settings, bystander-activated, nonviral

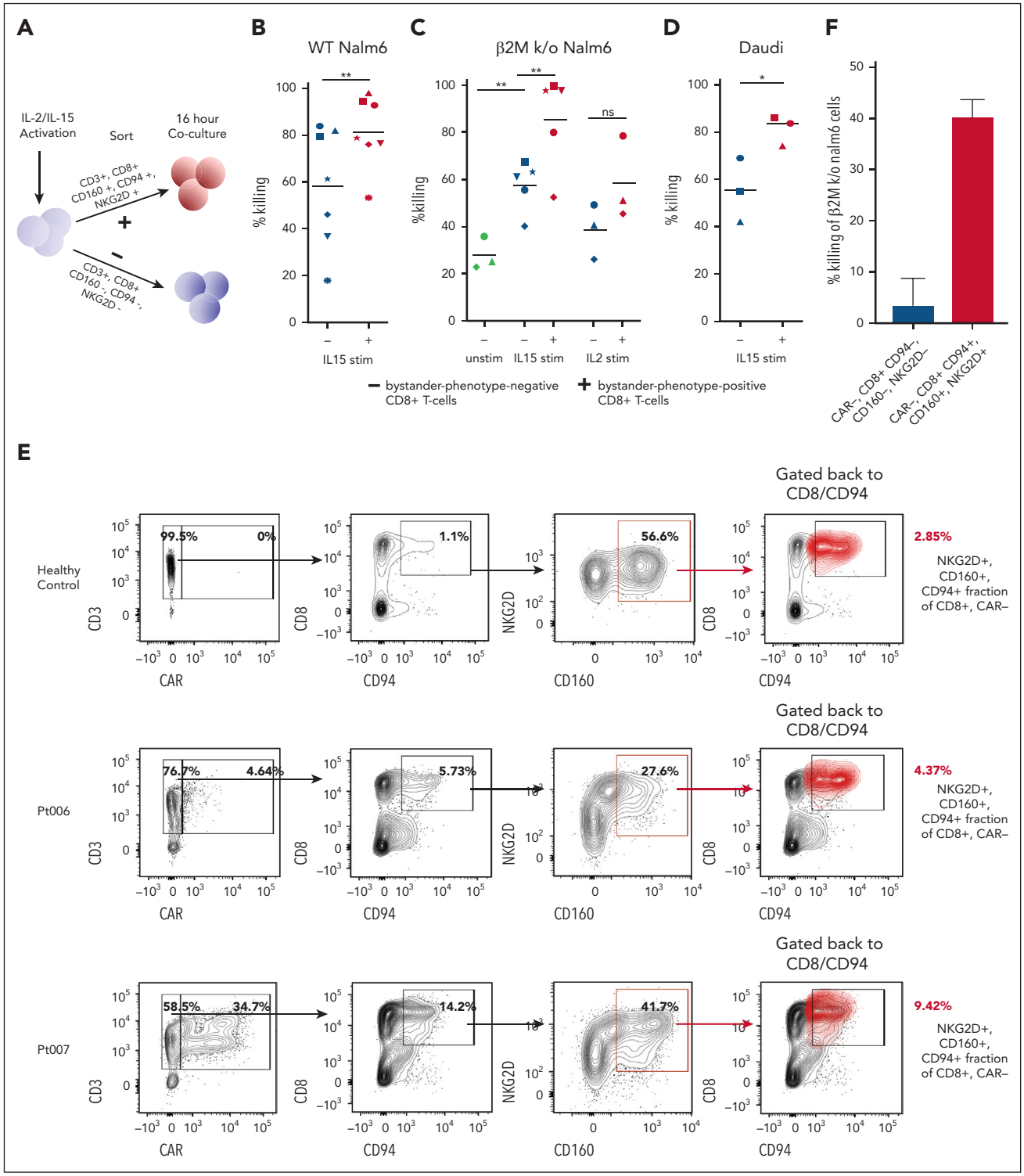


Figure 6. Cytokine-stimulated and patient–derived primary human bystander-phenotype-positive CD8⁺ T cells are capable of killing leukemia and lymphoma cell lines. (A) Schematic of coculture cytotoxicity assay. Cells were sorted for bystander-phenotype-positive and -negative CD8⁺ T cells and cocultured with Nalm6, β2M knockout Nalm6, or Daudi cells at effector-to-target ratio of 1:1 for 16 hours. (B) Percentage killing of Nalm6 (n = 7; paired *t* test) and (C) β2M knockout Nalm6 cells by unstimulated (n = 3; unpaired *t* test), IL-15 (n = 5; paired *t* test), and IL-2 (n = 3; paired *t* test)–stimulated bystander-phenotype-positive and -negative CD8⁺ T cells. (D) Percentage killing of Daudi cells after coculture with IL15-stimulated T cells sorted for bystander-phenotype-positive and -negative CD8⁺ T cells (n = 3; paired *t* test). Experiments were performed in duplicates or triplicates for each donor. Individual donors are represented by the unique symbols in the figure. (E) Frequency of CAR⁺ T cells and CD8⁺, CD94⁺, CD160⁺, and NKG2D⁺ CAR-negative T cells (red cluster) were determined by flow cytometric analysis in PBMCs isolated from a healthy donor, as well as from Pt006 and Pt007, with blood drawn 6 to 9 days after CAR T-cell infusion. (F) Percentage killing of β2M knockout Nalm6 cells 16 hours after coculture with bystander-phenotype-positive and -negative CD8⁺ T cells. This experiment was done with technical triplicates, the mean of all experiments is shown as ± standard error of mean. Stim, stimulated; unstim, unstimulated; WT, wild-type.

antigen-specific T cells were found to be CD8$^+$ effector T cells, which also demonstrated the expression of NK-cell markers and expression of cytolytic enzymes.[12-15,18,19,36,39,40] Bystander T cells of a similar phenotype have also been identified in solid tumors, and a recent report visualized activated T cells in lymphoma tissues after CAR T-cell infusion.[12,14,15] However, there is still a lack of comprehensive phenotypic and transcriptional analysis of activated bystander T cells in the context of CAR T-cell therapy. To address this gap, we used an NHP model for CAR T-cell therapy to investigate the activation of CAR^{neg} bystander cells. Patient-derived data sets for transcriptional analysis can be affected by various factors, such as the stage of the disease and prior treatments, making the NHP model an invaluable tool for this type of analysis. This model provided a consistent framework for identifying transcriptional patterns specific to bystander effects and enabled the discovery of a series of 4 bystander signatures, which subsequently served as the foundation for the identification and in-depth characterization of bystander-activated CAR^{neg} T cells in a cohort of patient samples. Although the expansion of CAR T cells in the NHP model is not dependent on the presence of malignant cells but rather on the presence of autologous B cells,[21] the NHP CAR T-cell model recapitulates CAR T-cell expansion and the associated release of inflammatory proteins and cytokines.[21] Despite the absence of malignant cells, we identified bystander-phenotype-positive CD8$^+$ T cells in the NHP model and demonstrated their similarity to bystander-phenotype-positive CD8$^+$ T cells in patients.

Bystander-activated T cells have been proposed to enhance both antiviral and antitumor immune responses.[13,14] This enhancement is thought to be partly mediated through TCR-independent cytotoxicity involving molecules such as NKG2D or the FAS cell surface death receptor (Fas)-FAS cell surface death receptor ligand (FasL) interaction.[16,18,40-42] Our experiments also confirmed the TCR-independent killing of leukemic cells. However, within the tumor microenvironment, some bystander-activated T cells may possess tumor antigen specificity and engage in TCR-dependent killing mechanisms. Although we did identify clonal expansions within the bystander population in the patient samples (in contrast to the NHP samples), the specificity of most of these clones could not be determined using public databases. The determination of whether these clones potentially possess antileukemic specificity remains an important area for future investigation.

We identified the gamma cytokine IL-15 as the major driver of in vitro differentiation of CD8$^+$ T cells toward bystander-phenotype-positive CD8$^+$ T cells. This finding suggests that ongoing clinical trials of CAR T cells that include the administration of IL-15, or the development of CAR T cells that autologously express this cytokine,[43-46] may have a salutary effect on bystander and CAR T cells.

Further investigations using large patient data sets to assess the association of bystander expansion with clinical response to CAR T cells will be required to validate the ability of these cells to enhance clinical tumor control. Our identification of a bystander signature that is amenable to both transcriptomic and flow cytometric assessments represents an important milestone toward conducting future analyses for this purpose.

Acknowledgments

This work was supported by funding from the National Institutes of Health (NIH), National Institute of Allergy and Infectious Diseases (NIAID) grant U19 AI1051731, NIH, National Heart, Lung, and Blood Institute (grants R01 HL095791, P01 HL158504, and P01 HL158505) and, NIH, NIAID U19 AI174967 (L.S.K.), the Helen Gurley Brown Presidential Initiative (U.G.), and the National Cancer Center Fellowship (U.G., J.K.).

Authorship

Contribution: J.K., U.G., L.S.K., and A.K.S. conceived the study; J.K., U.G., R.A.F., F.A-C., M.B.W., C.M., J.Z., E.E.H., F.E., X.R., V.T., and J.L. performed the experiments; P.K. and L.C. provided reagents; J.C., S.P.M., M.A.K., and S.H.C.B. provided patient samples and metadata; J.B.R., V.T., A.K.S., L.S.K., and U.G. provided feedback that helped frame key aspects of how the study was designed, conducted, and ultimately how the data were interpreted; and J.K., U.G., and L.S.K. wrote the manuscript, which was additionally commented on and edited by the remaining authors.

Conflict-of-interest disclosure: U.G. possesses intellectual property rights related to AlloVir, including interests in royalties. L.S.K. is on the scientific advisory board of Mammoth Biosciences and HiFiBIO; reports research funding from Magenta Therapeutics, Tessera Therapeutics, Novartis, Emmanuel Merck, Darmstadt Serono, Gilead Pharmaceuticals, and Regeneron Pharmaceuticals; reports consulting fees from Vertex; reports grants and personal fees from Bristol Myers Squibb; and the conflict-of-interest between L.S.K. with Bristol Myers Squibb is managed under an agreement with the Harvard Medical School. A.K.S. reports compensation for consulting and/or scientific advisory board membership from Merck, Honeycomb Biotechnologies, Cellarity, Repertoire Immune Medicines, Ochre Bio, Third Rock Ventures, Hovione, Relation Therapeutics, FL82, FL86, Empress Therapeutics, IntrECate Biotherapeutics, Senda Biosciences, and Dahlia Biosciences unrelated to this work. Parts of the study were supported by 2seventy bio. F.E. and E.E.H. are employees of 2seventy bio, J.B.R. is an employee of Tessara therapeutics, and S.P.M. is an employee of Cue Biopharma. The remaining authors declare no competing financial interests.

ORCID profiles: J.K., 0000-0002-5137-7516; F.A.-C., 0000-0001-5620-8431; X.R., 0009-0007-1219-4382; V.T., 0000-0001-6011-0576; A.K.S., 0000-0001-5670-8778.

Correspondence: Ulrike Gerdemann, Boston Children's Hospital/Dana-Farber Cancer Institute, 1 Blackfan Circle, Karp Research Building, 8th Floor 08004H, Boston, MA 02115; email: ulrike_gerdemann@dfci.harvard.edu.

Footnotes

Submitted 19 October 2023; accepted 16 March 2024; prepublished online on *Blood* First Edition 1 April 2024. https://doi.org/10.1182/blood.2023022717.

*A.K.S., L.S.K., and U.G. are joint senior authors.

Nonhuman primate and patient-derived single-cell RNA sequencing (scRNA-seq) data are available in the Gene Expression Omnibus database.

The online version of this article contains a data supplement.

The publication costs of this article were defrayed in part by page charge payment. Therefore, and solely to indicate this fact, this article is hereby marked "advertisement" in accordance with 18 USC section 1734.

REFERENCES

1. Frigault MJ, Maus MV. State of the art in CAR T cell therapy for CD19+ B cell malignancies. *J Clin Invest*. 2020;130(4):1586-1594.
2. Boyiadzis MM, Dhodapkar MV, Brentjens RJ, et al. Chimeric antigen receptor (CAR) T therapies for the treatment of hematologic malignancies: clinical perspective and significance. *J Immunother Cancer*. 2018;6(1):137.
3. Bachy E, Le Gouill S, Di Blasi R, et al. A real-world comparison of tisagenlecleucel and axicabtagene ciloleucel CAR T cells in relapsed or refractory diffuse large B cell lymphoma. *Nat Med*. 2022;28(10):2145-2154.
4. Fabrizio VA, Phillips CL, Lane A, et al. Tisagenlecleucel outcomes in relapsed/refractory extramedullary ALL: a pediatric real world CAR consortium report. *Blood Adv*. 2022;6(2):600-610.
5. Majzner RG, Mackall CL. Clinical lessons learned from the first leg of the CAR T cell journey. *Nat Med*. 2019;25(9):1341-1355.
6. Haradhvala NJ, Leick MB, Maurer K, et al. Distinct cellular dynamics associated with response to CAR-T therapy for refractory B cell lymphoma. *Nat Med*. 2022;28(9):1848-1859.
7. Wilson TL, Kim H, Chou CH, et al. Common trajectories of highly effective CD19-specific CAR T cells identified by endogenous T-cell receptor lineages. *Cancer Discov*. 2022;12(9):2098-2119.
8. Jackson Z, Hong C, Schauner R, et al. Sequential single-cell transcriptional and protein marker profiling reveals TIGIT as a marker of CD19 CAR-T cell dysfunction in patients with non-Hodgkin lymphoma. *Cancer Discov*. 2022;12(8):1886-1903.
9. Sheih A, Voillet V, Hanafi LA, et al. Clonal kinetics and single-cell transcriptional profiling of CAR-T cells in patients undergoing CD19 CAR-T immunotherapy. *Nat Commun*. 2020;11(1):219.
10. Deng Q, Han G, Puebla-Osorio N, et al. Characteristics of anti-CD19 CAR T cell infusion products associated with efficacy and toxicity in patients with large B cell lymphomas. *Nat Med*. 2020;26(12):1878-1887.
11. Anderson ND, Birch J, Accogli T, et al. Transcriptional signatures associated with persisting CD19 CAR-T cells in children with leukemia. *Nat Med*. 2023;29(7):1700-1709.
12. Chen PH, Lipschitz M, Weirather JL, et al. Activation of CAR and non-CAR T cells within the tumor microenvironment following CAR T cell therapy. *JCI Insight*. 2020;5(12):e134612.
13. Kim TS, Shin EC. The activation of bystander CD8(+) T cells and their roles in viral infection. *Exp Mol Med*. 2019;51(12):1-9.
14. Meier SL, Satpathy AT, Wells DK. Bystander T cells in cancer immunology and therapy. *Nat Cancer*. 2022;3(2):143-155.
15. Maurice NJ, Taber AK, Prlic M. The ugly duckling turned to swan: a change in perception of bystander-activated memory CD8 T cells. *J Immunol*. 2021;206(3):455-462.
16. Verneris MR, Karimi M, Baker J, Jayaswal A, Negrin RS. Role of NKG2D signaling in the cytotoxicity of activated and expanded CD8+ T cells. *Blood*. 2004;103(8):3065-3072.
17. Lerner EC, Woroniecka KI, D'Anniballe VM, et al. CD8(+) T cells maintain killing of MHC-I-negative tumor cells through the NKG2D-NKG2DL axis. *Nat Cancer*. 2023;4(9):1258-1272.
18. Chu T, Tyznik AJ, Roepke S, et al. Bystander-activated memory CD8 T cells control early pathogen load in an innate-like, NKG2D-dependent manner. *Cell Rep*. 2013;3(3):701-708.
19. Sottile R, Panjwani MK, Lau CM, et al. Human cytomegalovirus expands a CD8(+) T cell population with loss of BCL11B expression and gain of NK cell identity. *Sci Immunol*. 2021;6(63):eabe6968.
20. Tietze JK, Wilkins DE, Sckisel GD, et al. Delineation of antigen-specific and antigen-nonspecific CD8(+) memory T-cell responses after cytokine-based cancer immunotherapy. *Blood*. 2012;119(13):3073-3083.
21. Taraseviciute A, Tkachev V, Ponce R, et al. Chimeric antigen receptor T cell-mediated neurotoxicity in nonhuman primates. *Cancer Discov*. 2018;8(6):750-763.
22. Badia-I-Mompel P, Velez Santiago J, Braunger J, et al. decoupleR: ensemble of computational methods to infer biological activities from omics data. *Bioinform Adv*. 2022;2(1):vbac016.
23. Abbas AR, Wolslegel K, Seshasayee D, Modrusan Z, Clark HF. Deconvolution of blood microarray data identifies cellular activation patterns in systemic lupus erythematosus. *PLoS One*. 2009;4(7):e6098.
24. Kaech SM, Hemby S, Kersh E, Ahmed R. Molecular and functional profiling of memory CD8 T cell differentiation. *Cell*. 2002;111(6):837-851.
25. Lopez R, Regier J, Cole MB, Jordan MI, Yosef N. Deep generative modeling for single-cell transcriptomics. *Nat Methods*. 2018;15(12):1053-1058.
26. Lafi A, Parry JM. Cytogenetic activities of tobacco particulate matter (TPM) derived from a low to middle tar British cigarette. *Mutat Res*. 1988;201(2):365-374.
27. Gerdemann U, Fleming RA, Kaminski J, et al. Identification and tracking of alloreactive T cell clones in rhesus macaques through the RM-scTCR-seq platform. *Front Immunol*. 2021;12:804932.
28. Morisita M. Measuring of interspecific association and similarity between communities. Memoirs of the Faculty of Science, Kyushu Univ. 1959. *Series E (Biology)*. 1959;(3):65-80.
29. Gowthaman R, Pierce BG. TCR3d: the T cell receptor structural repertoire database. *Bioinformatics*. 2019;35(24):5323-5325.
30. Chronister WD, Crinklaw A, Mahajan S, et al. TCRMatch: predicting T-cell receptor specificity based on sequence similarity to previously characterized receptors. *Front Immunol*. 2021;12:640725.
31. Baumeister SHC, Mohan GS, Elhaddad A, Lehmann L. Cytokine release syndrome and associated acute toxicities in pediatric patients undergoing immune effector cell therapy or hematopoietic cell transplantation. *Front Oncol*. 2022;12:841117.
32. Diorio C, Shraim R, Myers R, et al. Comprehensive serum proteome profiling of cytokine release syndrome and immune effector cell-associated neurotoxicity syndrome patients with B-cell ALL receiving CAR T19. *Clin Cancer Res*. 2022;28(17):3804-3813.
33. Leem G, Jeon M, Kim KW, et al. Tumor-infiltrating bystander CD8(+) T cells activated by IL-15 contribute to tumor control in non-small cell lung cancer. *Thorax*. 2022;77(8):769-780.
34. Shin EC, Sung PS, Park SH. Immune responses and immunopathology in acute and chronic viral hepatitis. *Nat Rev Immunol*. 2016;16(8):509-523.
35. Maini MK, Boni C, Lee CK, et al. The role of virus-specific CD8(+) cells in liver damage and viral control during persistent hepatitis B virus infection. *J Exp Med*. 2000;191(8):1269-1280.
36. Sckisel GD, Tietze JK, Zamora AE, et al. Influenza infection results in local expansion of memory CD8(+) T cells with antigen non-specific phenotype and function. *Clin Exp Immunol*. 2014;175(1):79-91.
37. Doisne JM, Urrutia A, Lacabaratz-Porret C, et al. CD8+ T cells specific for EBV, cytomegalovirus, and influenza virus are activated during primary HIV infection. *J Immunol*. 2004;173(4):2410-2418.
38. Bangs SC, McMichael AJ, Xu XN. Bystander T cell activation–implications for HIV infection and other diseases. *Trends Immunol*. 2006;27(11):518-524.
39. Klampatsa A, Leibowitz MS, Sun J, Liousia M, Arguiri E, Albelda SM. Analysis and augmentation of the immunologic bystander effects of CAR T cell therapy in a syngeneic mouse cancer model. *Mol Ther Oncolytics*. 2020;18:360-371.
40. Zhang X, Zhang Y, Liu H, et al. IL-15 induced bystander activation of CD8(+) T cells may mediate endothelium injury through NKG2D in Hantan virus infection. *Front Cell Infect Microbiol*. 2022;12:1084841.
41. Upadhyay R, Boiarsky JA, Pantsulaia G, et al. A critical role for Fas-mediated off-target

tumor killing in T-cell immunotherapy. *Cancer Discov*. 2021;11(3):599-613.

42. Hong LK, Chen Y, Smith CC, et al. CD30-redirected chimeric antigen receptor T cells target CD30(+) and CD30(-) embryonal carcinoma via antigen-dependent and Fas/FasL interactions. *Cancer Immunol Res*. 2018;6(10):1274-1287.

43. Ataca Atilla P, McKenna MK, Tashiro H, et al. Modulating TNFalpha activity allows transgenic IL15-Expressing CLL-1 CAR T cells to safely eliminate acute myeloid leukemia. *J Immunother Cancer*. 2020;8(2):e001229.

44. Mu-Mosley H, Ostermann L, Muftuoglu M, et al. Transgenic expression of IL15 retains CD123-redirected T cells in a less differentiated state resulting in improved anti-AML activity in autologous AML PDX models. *Front Immunol*. 2022;13:880108.

45. Heczey A, Xu X, Courtney AN, et al. Anti-GD2 CAR-NKT cells in relapsed or refractory neuroblastoma: updated phase 1 trial interim results. *Nat Med*. 2023;29(6):1379-1388.

46. Hirayama AV, Chou CK, Miyazaki T, et al. A novel polymer-conjugated human IL-15 improves efficacy of CD19-targeted CAR T-cell immunotherapy. *Blood Adv*. 2023;7(11):2479-2493.

© 2024 American Society of Hematology. Published by Elsevier Inc. All rights are reserved, including those for text and data mining, AI training, and similar technologies.